Electronic Supplementary Information (ESI)

Title: Polarization-independent broadband meta-holograms via polarization-dependent nanoholes

Xiaohu Zhang,[a,b,#] Xiong Li,[a,#] Jinjin Jin,[a,b] Mingbo Pu,[a] Xiaoliang Ma,[a] Jun Luo,[a] Yinghui Guo,[a] Changtao Wang,[a] and Xiangang Luo*[a]

[a.] State Key Lab of Optical Technologies on Nano-Fabrication and Micro-Engineering, Institute of Optics and Electronics, Chinese Academy of Sciences, P.O. Box 350, Chengdu, 610209, China. E-mail: lxg@ioe.ac.cn.

[b.] University of Chinese Academy of Sciences, Beijing 100049, China.

[#]These authors contributed equally to this work.

1. The design of 2D polarization-independent hologram for arbitrary picture

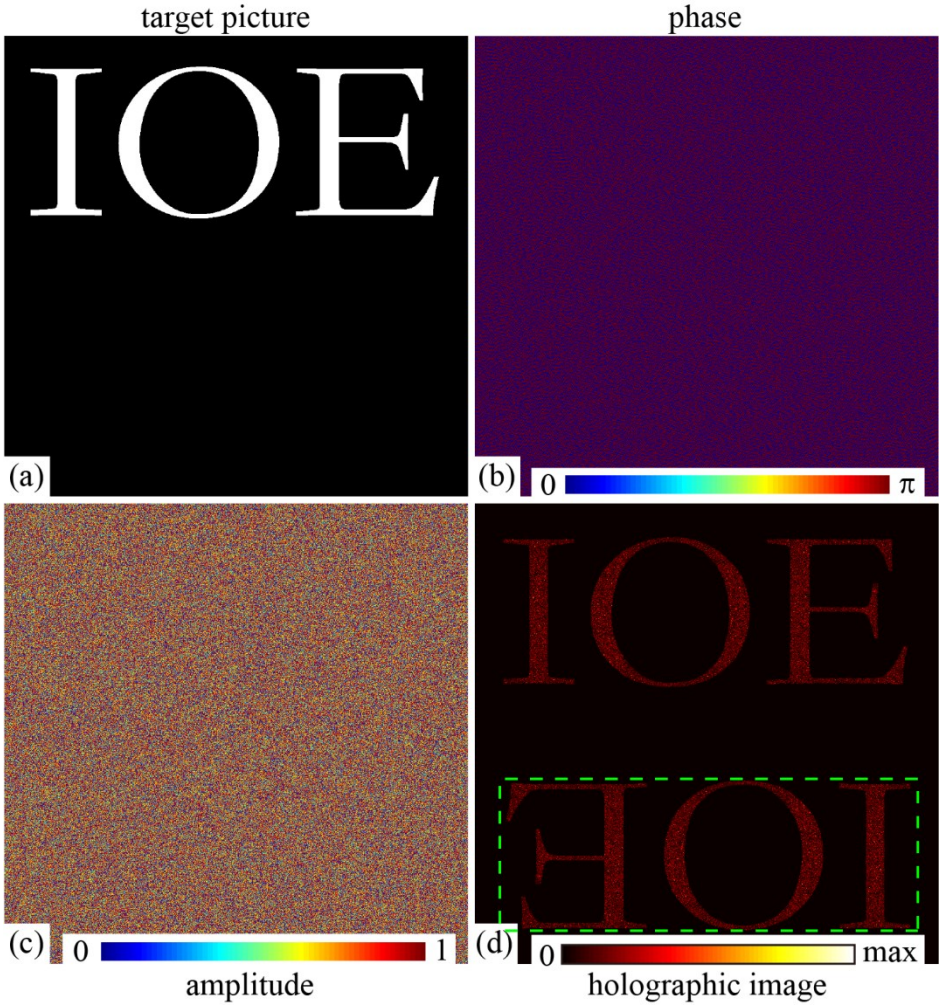

Figure S1: (a) The target picture of the letter "IOE" for the 2D polarization-independent hologram. (b) The phase and (c) amplitude distributions of the designed complex amplitude hologram. (d) The simulation holographic image of the designed polarization-independent hologram.

For designing polarization-independent 2D hologram of arbitrary target picture, we let the target picture in half of the frequency spectrum of the hologram to eliminate the interference between the target image and the conjugate image. As shown in Figure S1 (a), the letter "IOE" is located in top half of the frequency spectrum of the hologram. The last complex amplitude hologram is achieved by extracting the real part of the phase hologram $e^{i\phi(x_0,y_0)}$ calculated by the IFTA and its phase and amplitude are shown in Figure S1 (b) and (c), respectively. The simulation holographic image of the designed complex amplitude when setting the incident light with linear polarization is shown in Figure S1 (d). The part of the holographic image in the green dashed line is the conjugate image of the preset target picture. It's visually illustrated that half of the energy and frequency spectrum information are wasted as a result of the conjugate image. So the centrosymmetric snowflake picture is used as the target picture of the 2D hologram in the experiment, as demonstrated in the main text.

2. The theoretical analysis for different polarizations light incidence

We first analyze the case of the 2D hologram for noncenter-symmetric target. The incident light is assumed as a plane wave with the amplitude A_0. The target image intensity distribution is $I(f_x,f_y)$ in the Fraunhofer region of the phase hologram (phase distribution $\phi(x_0,y_0)$), which is achieved by iterative Fourier-transform (IFTA) algorithm. Then we can obtain the relation:

$$\mathrm{I}\left(f_x, f_y\right)=A_0^{\,2}\left|F(\mathrm{e}^{i\phi(x_0,y_0)})\right|^2 \tag{1}$$

$$\mathrm{I}\left(-f_x, -f_y\right)=A_0^{\,2}\left|F(\mathrm{e}^{-i\phi(x_0,y_0)})\right|^2 \tag{2}$$

Where (x_0,y_0) and (f_x,f_y) are the coordinate of the fabricated hologram and its frequency spectrum, respectively. The F represents the Fourier transformation. The distribution of $\cos(\phi(x_0,y_0))$ is used as our polarization-independent complex amplitude hologram, which is achieved by superimposing the $e^{i\phi(x_0,y_0)}$ and $e^{-i\phi(x_0,y_0)}$. The complex amplitude-angle relation of $\sin(2\theta)$ with x-polarization incident light is used to code the complex amplitude hologram. So the value of θ is decided by:

$$\theta=\frac{\pi}{4}-\frac{\phi(x_0,y_0)}{2},(0<\phi(x_0,y_0)\le\pi) \tag{3}$$

$$\theta=-\frac{3\pi}{4}+\frac{\phi(x_0,y_0)}{2},(\pi<\phi(x_0,y_0)\le 2\pi) \tag{4}$$

As x-polarization light impinges on the fabricated meta-hologram, the intensity distribution of the image plane is:

$$\begin{aligned}\mathrm{I}'\left(f_x, f_y\right)&=A_0^{\,2}\left|F(\sin(2\theta))\right|^2=A_0^{\,2}\left|F(\cos(\phi(x_0,y_0)))\right|^2\\&=0.25A_0^{\,2}\left|F(\mathrm{e}^{i\phi(x_0,y_0)})+F(\mathrm{e}^{-i\phi(x_0,y_0)})\right|^2\\&=0.25\left[\mathrm{I}\left(f_x, f_y\right)+\mathrm{I}\left(-f_x, -f_y\right)+A_0^{\,2}F(\mathrm{e}^{i\phi(x_0,y_0)})(F(\mathrm{e}^{-i\phi(x_0,y_0)}))^*+A_0^{\,2}(F(\mathrm{e}^{i\phi(x_0,y_0)}))^*F(\mathrm{e}^{-i\phi(x_0,y_0)})\right]\end{aligned} \tag{5}$$

Theoretically, the value of the third item of equation (5), $0.25A_0^2F(e^{i\phi(x_0,y_0)})$ $F(e^{-i\phi(x_0,y_0)})^*$,is 0 because of the target image, coming from $F(e^{i\phi(x_0,y_0)})$, is located in half of the frequency spectrum of the hologram and its conjugate image, coming from $F(e^{-}$

$e^{i\phi(x_0,y_0)}$), is in the other half of the frequency spectrum, as shown in Figure S1 (a) and (d). The fourth item value is 0 for the same reason. The equation (5) is coordinated with the results shown in Figure S1. The first item is $0.25\cdot I(f_x,f_y)$, which indicates the target image can be achieved with *x*-polarization incident light.

If the *x*-polarization is changed into *y*-polarization, then:

$$I''(f_x,f_y)=A_0^2\left|F(\sin(2(\theta-\frac{\pi}{2})))\right|^2=A_0^2\left|F(-\sin(2\theta))\right|^2=I'(f_x,f_y) \tag{6}$$

From equation (6), we can conclude that the holographic image achieved with y-polarization incident light is the same for x-polarization. In theory, a certain polarization is composed of different components of x-polarization and y-polarization. Consequently, same holographic image will be achieved with other polarizations light incidence on the sample. In addition, the depolarized light can be seen as a series of light beams with different linear polarizations. Therefore, the holographic images with same profile would be fulfilled with those linearly polarized light beams incidence. The last holographic result is the superimposition of those images. Nevertheless, the holographic image of the depolarized light is much dimmer than the results with x-polarization or y-polarization incidence with setting the same incident power duo to the partially coherent feature of those light beams, which is in accord with the results shown in Figure 4f-h.

For the incident circularly polarized light, the geometric phase $\mathcal{E}=2\sigma\theta$ should be considered, where $\sigma=\pm1$ denotes the LCP/RCP incident light. Here we assume that the incident polarization is LCP, thus, the image intensity can be expressed as:

$$I'''(f_x,f_y)=A_0^2\left|F(e^{i2\theta})\right|^2=A_0^2\left|F(e^{i2(\frac{\pi}{4}-\frac{\phi(x_0,y_0)}{2})})\right|^2\approx\frac{1}{4}\cdot I(-f_x,-f_y),(0<\phi(x_0,y_0)\le\pi)$$

$$=A_0^2\left|F(e^{i2(-\frac{3\pi}{4}+\frac{\phi(x_0,y_0)}{2})})\right|^2\approx\frac{1}{4}\cdot I(f_x,f_y),(\pi<\phi(x_0,y_0)\le2\pi) \tag{7}$$

The quantity of the $\phi(x_0,y_0)$ value in the range from 0 to π is approximately equal to that in the range of π to 2π. Therefore, the amplitudes of the target image and conjugate image of polarization-independent hologram are about 1/2 time to the original amplitude of the holographic image of the IFTA. So the intensity coefficient $(1/2)^2=1/4$ would be achieved, as shown in equation (7). This equation indicates the target holographic image can be achieved with LCP light incidence.

While the incident polarization is changed into RCP, the image intensity becomes:

$$I''''(f_x,f_y)=A_0^2\left|F(e^{-i2\theta})\right|^2=A_0^2\left|F(e^{-i2(\frac{\pi}{4}-\frac{\phi(x_0,y_0)}{2})})\right|^2\approx\frac{1}{4}\cdot I(f_x,f_y),(0<\phi(x_0,y_0)\le\pi)$$

$$=A_0^2\left|F(e^{-i2(-\frac{3\pi}{4}+\frac{\phi(x_0,y_0)}{2})})\right|^2\approx\frac{1}{4}\cdot I(-f_x,-f_y),(\pi<\phi(x_0,y_0)\le2\pi) \tag{8}$$

We can conclude from equations (7)-(8) that the target image $I(f_x,f_y)$ can be implemented with both LCP and RCP incident light even though half of the energy is

sacrificed for the conjugate image. With LCP incident light, the target holographic mage is achieved with the pixels with phase $\phi(x_0,y_0)$ in the range from π to 2π, while the corresponding image is realized using the phase $\phi(x_0,y_0)$ in the range from 0 to π with RCP incident light. That is to say, the target image intensity of LCP and RCP incident light are not entirely equal. However, the discrepancy is very small and can be neglected since the pixel quantity in those two ranges is approximately equal, especially when the hologram contains abundant of pixels. For example, the intensity discrepancy of the target images with LCP and RCP light incidence for the design shown in Section 1 of ESI is about 0.00012 time to the total intensity of target image. So little discrepancy cannot be measured in our experiment. In addition, the profiles of the target holographic images are always identical. The theoretical analysis shown in equations (5)-(8) indicates the polarization-independent character of the 2D meta-hologram designed by our proposed algorithm. The theoretical analysis of the 3D polarization-independent hologram is similar to the case of 2D hologram, so we don't show it here again.

3. **The experimental results of 2D hologram for different polarizations**

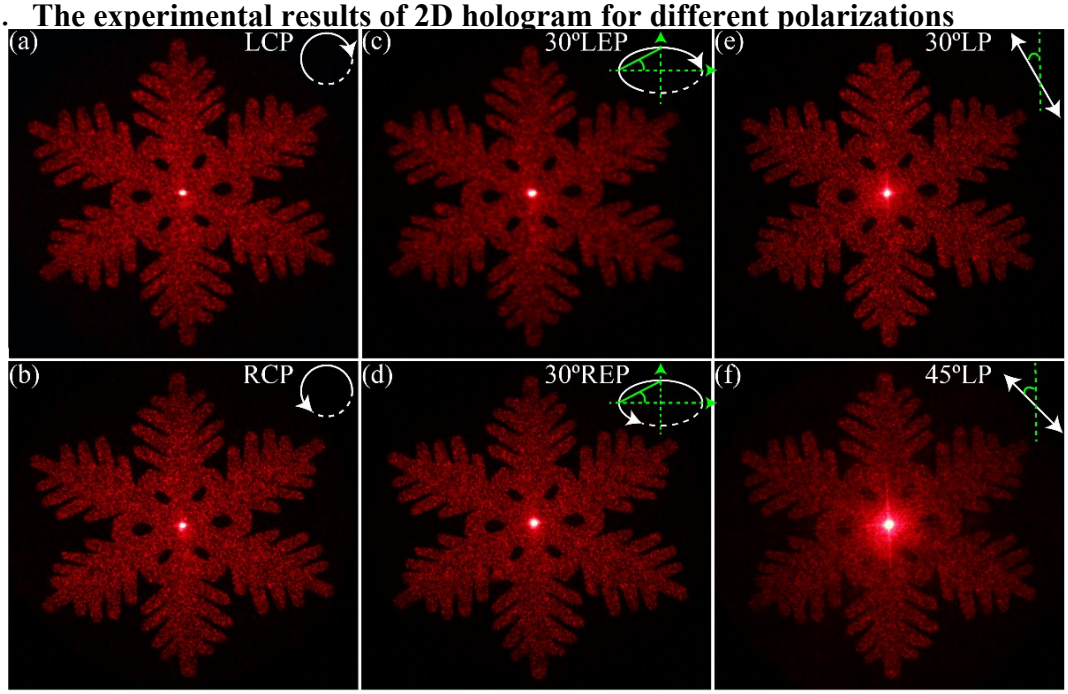

Figure S2: The experimental holographic image for incident (a) LCP, (b) RCP, (c) 30° LEP, (d) 30° REP, (e) 30° linear polarization and (f) 45° linear polarization light. LCP: left circular polarization, RCP: right circular polarization, LEP: left ellipse polarization, REP: right ellipse polarization.

For further verifying the polarization-independent property of our fabricated sample, other different polarizations light, such as LCP (left circular polarization), RCP (right circular polarization), LEP (left ellipse polarization), REP (right ellipse polarization) and linear polarization light, is used to illuminate the meta-hologram. The corresponding experimental results for LCP, RCP, 30°LEP and 30°REP light are shown in Figure S2 (a)-(d), respectively. The related angles for the 30° are marked in

Figure S2 (c) and (d), which means the long axis length is $\sqrt{3}$ times to short axis length of the polarization trajectory ellipse. It should be noted that the LP_2 (Figure 4e) is removed and a QWP_2 (quarter wave plate) is added between the sample and LP_3 in the experimental setup, which is similar to the experiment setup shown in Figure 3e. The different CP (circular polarization) and EP (ellipse polarization) light are achieved by rotating the orientation angle of the QWP and the noise is filtered by the pair of QWP_2 and LP_3. Figure S2 (e) and (f) show the holographic images for linear polarization light, whose orientation angles between the polarization orientation and vertical direction are 30° and 45°, respectively. The experimental results shown in Figure S2 further prove the feasible of the proposed algorithm for realizing the polarization-independent holographic image.

4. The results of another design of 3D polarization-independent hologram

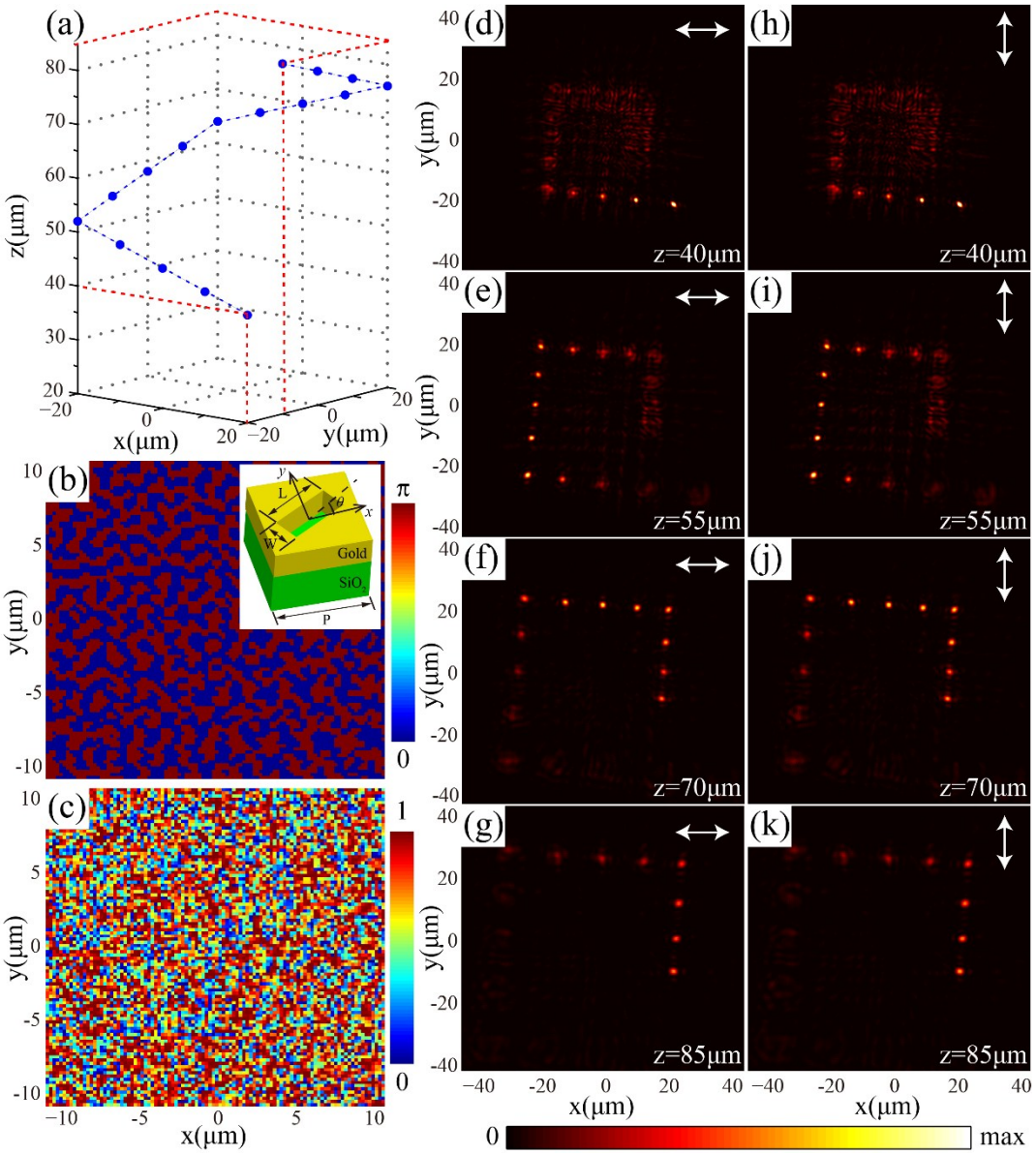

Figure S3: (a) Schematic diagram of the 3D target object, which is consisted of

sixteen points in different position. The phase (b) and amplitude (c) distribution of the designed hologram (100×100 pixels, 20μm×20μm). The coding structure is shown in the inset of Figure (b) with the size: P=200nm (period), L=140nm (length), W=60nm (width). θ: the orientation angle of the elongated aperture. The thickness of the gold film is 120nm. The substrate is SiO_2. (d)-(g) The simulation results of the holographic image with different distances in the z-axis with x-polarization light incidence using CST software. (h)-(k) The corresponding simulation results with y-polarization light incidence. The incident wavelength is set with 405nm.

For further verifying the feasibility of the proposed algorithm for 3D image, we design another 3D hologram for the target object shown in Figure S3 (a). The target object is consisted of sixteen points with different coordinates in x/y/z-axis. We firstly use the point source algorithm[1, 2] to achieve the phase-only hologram (phase distribution $\phi(x_0,y_0)$) and the polarization-independent complex amplitude hologram $\cos(\phi(x_0,y_0))$ is obtained by extracting the real part of $e^{i\phi(x_0,y_0)}$. The phase and amplitude distributions of the designed 3D polarization-independent hologram are shown in Figure S3 (b)-(c). The elongated aperture used to code the hologram is shown in the inset of Figure S3 (b). The period (P=200nm), length (L=140nm) and width (W=60nm) are shown in the figure. The phase and amplitude of the hologram are controlled by changing the orientation angle (θ) with the amplitude-angle relation $|\sin(2\theta)|$ and phase-angle relation. More information about the used structure can be found in other works.[2-4] The reason for using the elongated aperture with period 200nm other than elliptical nanohole with period 350nm is decreasing the computation load with the same pixels in the CST Microwave Studios. The open boundary conditions are used along x, y and z directions in the full model simulation with CST software. The electromagnetic field distribution on the plane with a distance 0.3μm away from the metasurface is calculate by CST software and the electric field distribution on other planes are simulated by using Fresnel diffraction theory. The simulation holographic images of several transections with different distance along z-axis with x-polarization and y-polarization incidence are shown in Figure S3 (d)-(g) and (h)-(k), respectively. With 2D results on different plane, the 3D feature of the 3D image is verified. The holographic images shown Figure S3 (d)-(g) match well with the results shown in Figure S3 (h)-(k), which further demonstrated the proposed algorithm is feasible for designing real 3D polarization-independent hologram.

1. L. Huang, X. Chen, H. Mühlenbernd, H. Zhang, S. Chen, B. Bai, Q. Tan, G. Jin, K. W. Cheah, C. W. Qiu, J. Li, T. Zentgraf and S. Zhang, *Nat. Commun.*, 2013, **4**, 2808.
2. X. Zhang, J. Jin, M. Pu, X. Li, X. Ma, P. Gao, Z. Zhao, Y. Wang, C. Wang and X. Luo, *Nanoscale*, 2016, **9**, 1409-1415.
3. L. Liu, X. Zhang, M. Kenney, X. Su, N. Xu, C. Ouyang, Y. Shi, J. Han, W. Zhang and S. Zhang, *Adv. Mater.*, 2014, **26**, 5031-5036.
4. D. Tang, C. Wang, Z. Zhao, Y. Wang, M. Pu, X. Li, P. Gao and X. Luo, *Laser*

Photonics Rev., 2015, **9**, 713-719.